ECS Journal of Solid State
Science and Technology

Nanoindentation and Photoluminescence Studies of Hydrogenated Boron Carbon Nitride Thin Films

ECS Journal of Solid State Science and Technology, 2021 **10** 057004

Nanoindentation and Photoluminescence Studies of Hydrogenated Boron Carbon Nitride Thin Films

Shraddha Dhanraj Nehate,[1,*,z] Ashwin Kumar Saikumar,[1] Mustafa Fincan,[2] Anthony Santana,[3] Alex A Volinsky,[2] Andres Campiglia,[3] and Kalpathy B. Sundaram[1,]**

[1]*Department of Electrical and Computer Engineering, University of Central Florida, Orlando, FL, 32816, United States of America*
[2]*Department of Mechanical Engineering, University of South Florida, Tampa, Florida 33620, United States of America*
[3]*Department of Chemistry, University of Central Florida, Orlando, Florida 32816, United States of America*

Nanoindentation and photoluminescence (PL) studies were performed on hydrogenated boron carbon nitride thin films deposited using radio frequency magnetron sputtering. Dual target sputtering from B_4C and BN targets was used to deposit films. The variation in the composition of films was studied using energy-dispersive X-ray spectroscopy. The influence of hydrogen gas and substrate temperature on the mechanical properties was investigated using nanoindentation measurements. Photoluminescence studies were performed on films deposited under varying hydrogen content and different deposition temperatures. The films deposited in this study exhibited hardness of 6–22 GPa and Young's modulus of 125–140 GPa. PL spectra demonstrated two prominent emission peaks around 499 nm and 602 nm for the deposited films. Increasing the hydrogen gas ratio in the films induced PL peak shifts to longer wavelengths. Emission spectra shifted to long wavelength with increasing substrate temperature. The emission peak position shifted from 499 nm to 544 nm and from 602 nm to 655 nm as a function of substrate temperature. For the first time, BCNH based thin films PL behavior at low temperature (77 K) has been characterized in this study. The BCNH thin films show a rare phenomenon of negative thermal quenching of emission.
 [DOI: 10.1149/2162-8777/abf8fc]

Manuscript submitted January 27, 2021; revised manuscript received March 28, 2021. Published May 12, 2021.

Boron nitride (BN) consisting of boron-nitrogen covalent bonds exists in three crystalline forms as hexagonal (h-BN), cubic (c-BN), and rarely found wurtzite (w-BN) phases. The h-BN material has a structure analogous to graphite with high chemical and thermal stability, non-toxicity. It has been widely used as an electrical insulator, heat-resistant refractory material, and interface coatings for high-temperature ceramic matrix composites.[1,2] While the diamond is the hardest material, c-BN is next to diamond in terms of hardness and has high thermal stability with high abrasive wear resistance and hence finds application in cutting tools.[3] h-BN has been regarded as a promising material for the potential ultraviolet light source and optoelectronic applications owing to its wide bandgap.[4] The structural similarity between graphite and h-BN stimulated research on hybrid boron carbon nitrogen (BCN) materials.

The unique properties of graphite and boron nitride are combined in BCN compounds, and these properties can be tuned depending on the composition and structure. As graphite is semi-metallic and h-BN is insulating, hybrid BCN between graphite and h-BN exhibits semiconducting properties. Several other methods for depositing BCN thin films, such as chemical vapor deposition,[5,6] radio frequency (RF) and direct current (DC) magnetron sputtering,[7,8] pulsed laser deposition,[9] and ion beam assisted deposition,[10] have been reported in the literature. Boron carbon nitride materials continue to be explored due to their unique properties, such as low dielectric constant, exceptional chemical inertness, outstanding thermal and mechanical strength, along with transparency in optical and UV ranges.[11–16] These excellent properties of BCN multi-functional materials allowed their applications as anti-wear and protective coatings,[17,18] energy storage,[19,20] supercapacitors,[21,22] UV detectors,[15] nanobiotechnology and nanomedicine.[23,24]

Nitride-based phosphors have attracted attention because of their favorable properties, such as non-toxicity, good thermal and chemical stability, the broad range of excitation and emission wavelengths, and luminescence efficiency upon activation using rare-earth ions.[25–27] However, these materials require high temperatures and pressure. BCN films deposited by RF sputtering do not require such conditions. As a result, BCN materials with variable energy bandgap are being explored for their vital role in developing new, environmentally friendly luminescent devices.[28–30]

The addition of small amounts of hydrogen gas has been proven beneficial for improving the electrical and optical properties of BCN films.[31–33] Mechanical properties and luminescence of BCN films deposited using RF sputtering have been previously reported.[34,35] This study aims to investigate the changes in mechanical properties and photoluminescence with the addition of hydrogen gas and varying substrate deposition temperature using dual-target RF sputtering. The sputtering technique provides the freedom to select substrate material and achieves uniform film deposition. Additionally, the dual-target approach offers the ability to tune film composition based on the deposition parameters. BCN films were deposited by dual-target B_4C and BN sputtering in the presence of varying hydrogen, N_2 gasses, and deposition temperature. The chemical composition, chemical bonding, hardness, Young's modulus, and photoluminescence (PL) properties of BCN films were investigated. For the first time, BCNH phosphors with a red emission peak, which can reach 655 nm are reported.

Materials and Methods

Deposition of BCN thin films.—BCN thin films were deposited by dual-target RF sputtering using B_4C and BN targets in the AJA International ultra-high vacuum sputtering system. Both targets used were powder pressed with a three-inch diameter and 99.5% purity. The sputtering system was evacuated to a base pressure of $\sim 4 \times 10^{-7}$ Torr before deposition. Hydrogen-argon (3% hydrogen, 97% argon) and nitrogen were the two types of working gases used. Since hydrogen gas introduced into the deposition chamber is premixed with argon, it will henceforth be referred to as H_2Ar. The H_2Ar to nitrogen ($H_2Ar + N_2$) gas flow ratio was varied from 0 to 1 in steps of 0.2, while the total gas flow to the chamber was set to 20 sccm. To study the effects of substrate temperature on mechanical properties and PL, BCN films were deposited at varying substrate temperature from room temperature (RT) to 400 °C with a constant H_2Ar to ($H_2Ar + N_2$) ratio of 1. Identical sputtering power of 200 W was provided to both B_4C and BN targets, while the deposition pressure was maintained at 5 mTorr. Oxidized silicon wafers (~4000 Å oxide

*Electrochemical Society Student Member.
**Electrochemical Society Fellow.
[z]E-mail: shraddha.nehate@knights.ucf.edu

Table I. Varying hydrogen gas flow and substrate temperature used to deposit BCN films.

Film	$H_2Ar/(H_2Ar+N_2)$	H_2Ar	N_2	Deposition Temperature
A	0	0	20	RT
B	0.2	4	16	RT
C	0.4	8	12	RT
D	0.6	12	8	RT
E	0.8	16	4	RT
F	1.0	20	0	RT
G	1.0	20	0	100 °C
H	1.0	20	0	200 °C
I	1.0	20	0	300 °C
J	1.0	20	0	400 °C

thickness) and glass substrates were used to deposit BCN thin films. These substrates were cleaned by rinsing with acetone, methanol, deionized water, and blow-dried with nitrogen. The substrates were placed on a rotating substrate holder with a rotation speed set to 20 rpm to achieve uniform films. Both targets face the substrate holder at an angle of 45°. Table I shows gas flow ratio computations for all films deposited at 5mTorr at the total gas flow of 20 sccm.

Surface characterization.—BCNH films deposited on oxidized silicon wafers were used to measure elemental composition, mechanical properties, and PL emissions. The elemental composition of the films was determined using the energy-dispersive X-ray spectroscopy (EDS). EDS data was processed using the Thermo Scientific™ NORAN™ system 7. Glass substrates were used to measure the thickness of BCN films deposited on them. The thickness of the BCN thin films, which ranged between 2000 Å and 3000 Å was measured using Dektak 150 stylus profilometer (Veeco, USA). Double side polished p-type silicon wafers were used to deposit films to identify chemical bonding using the Fourier Transform Infrared Spectroscopy (FTIR). FTIR transmission spectra were recorded using the Jasco FT/IR 6600 spectrometer equipped with a Ge/KBr beam splitter. A DLaTGS (deuterated lanthanum α-alanine doped triglycine sulfate) detector was used for the spectral measurements. Transmission FTIR spectra were collected from 400–4000 cm^{-1} with a resolution of 4 cm^{-1}.

Mechanical properties of the films were characterized using a Hysitron TriboIndenter (Hysitron, USA) equipped with a Berkovich diamond tip. Indentation time was 4 s for loading and 4 s for unloading steps. Measurements were performed with a fixed distance of 30 μm between two neighboring indents. Multiple indentations were made for each film at a constant maximum load of 4 mN. Values obtained were averaged for each film.

The PL measurements were performed using a FluoroMax-3 equipped with a 150 W Xenon arc lamp as the light source. The measurements were performed at RT and 77 K. Measurements were made on a custom fiber optic probe (FOP) using two excitation fibers and eight emission fibers in an 8 around 2 configurations. The fibers were held in a copper tube, which provided mechanical support for immersing the sample in cryogens.

Results and Discussion

Elemental composition.—EDS was conducted for elemental composition analysis of the BCN films. EDS analysis identified boron, carbon, nitrogen, and oxygen elements in the films. The film composition varies depending on the synthesis conditions shown in Fig. 1. An initial increase in H_2Ar caused a slight decrease in the boron composition. However, a further increase in H_2Ar gas increased the boron concentration to a maximum of 33.4% at the $H_2Ar/(H_2Ar + N_2)$ ratio of 1. Varying gas flow caused dramatic variation in the nitrogen concentration in the film. The nitrogen concentration was 35% at $H_2Ar/(H_2Ar + N_2)$ ratio of 0 and subsequently decreased with increasing ratio with an exception of $H_2Ar/(H_2Ar + N_2) = 0.8$ when the nitrogen concentration was recorded to be 24.4%. As expected, the nitrogen content was highest when the gas ratio was 0, which means when N_2 was solely used as the sputtering gas in the absence of H_2Ar. It is interesting to observe that the carbon concentration in BCN films did not vary significantly with changes in gas ratio. The oxygen content seems to be high in the films. The reduction of oxygen content in the film with gas ratio of 1 is compensated by the increase in boron content. The oxygen incorporation may have occurred during the post-processing of samples in the air. BCN films processed with hydrogen gas have been reported to contain large amounts of oxygen due to low porosity.[36] The variability in the composition is critical for the BCN films, since the composition alterations govern the film properties.

BCN films deposited at the $H_2Ar/(H_2Ar + N_2)$ ratio of 1 with different substrate temperatures displayed a different relationship between the elemental concentration, as shown in Fig. 1b. With increasing deposition temperature, the boron content did not change up to 300 °C, beyond which there was a slight reduction in boron content in the films deposited at 400 °C. On the contrary, the carbon concentration sightly increased from RT to 400 °C. The nitrogen

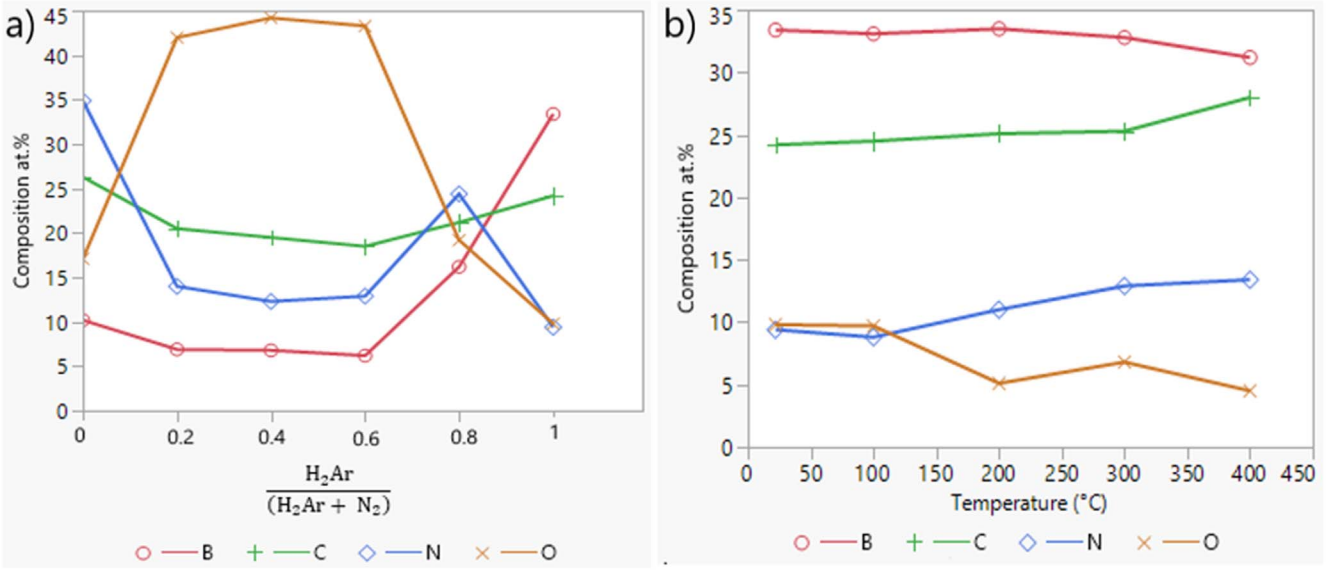

Figure 1. Composition data obtained from EDS for films with (a) varying gas flow ratios (b) varying substrate temperature.

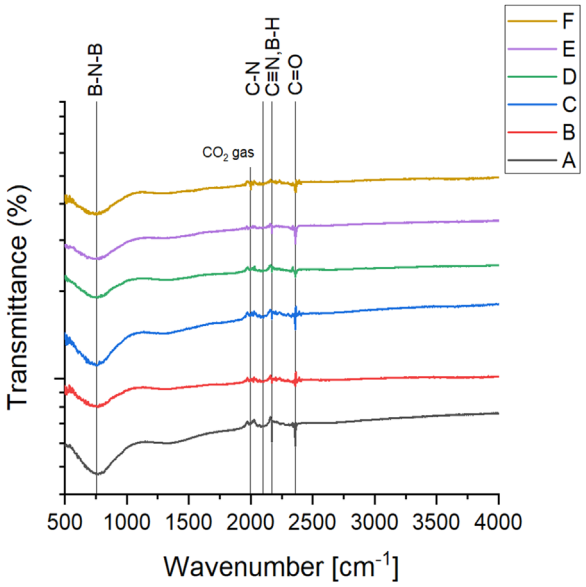

Figure 2. FTIR transmittance spectra of BCNH thin films deposited at varying gas flow.

concentration gradually increased with deposition temperature. With varying deposition temperature, the atomic composition in the films shows minimal variation, revealing that under current experimental conditions, the chemical composition of BCN films is not highly sensitive to substrate temperature in the investigated range.[36,37] Oxygen content remained relatively low when films were deposited at the substrate temperature. In these measurements, hydrogen concentration is not taken into consideration.

Chemical bonding.—FTIR was performed to recognize the functional groups present in the films. Since films deposited with varying gas ratios (Film A-F) demonstrated high oxygen content, FTIR was performed on these films to recognize the chemical bonding. Figure 2 shows FTIR transmission spectra of as-deposited films with varying H_2/Ar to N_2 gas ratios. The peak at 2360 cm^{-1} is attributed to C=O.[38] As supported by the EDS, oxygen in the films seems to bond with carbon. The peak at 2170 cm^{-1} could be attributed to C≡N and B-H formations in the films. This peak is distinct for film A, gradually decreases for films B to E, and tends to disappear for film F. This indicates a transition of phase in the films with varying gas ratios and is consistent with prior reports.[34] The broad peak at 2100 cm^{-1} is typically assigned to C–N.[35] It is noteworthy that film A exhibited a clear C–N peak; however, the intensity reduced with the hydrogen gas ratio. Such an interpretation would imply that pure BCN films predominantly exhibit strong C–N bonding, but the films undergo phase transitions with varying gas ratios. The absorption peak observed just below 2000 cm^{-1} is likely due to background CO_2 gas in the FTIR spectrometer. The broad band stretching from 500 cm^{-1} to 1000 cm^{-1} with a peak at 750 cm^{-1} is attributed to out-of-plane sp^2 bonded B-N-B bending mode.[15,39] No evidence of N–H and O–H peaks in the range of 3300–3600 cm^{-1} was found in the spectrum.

Nanoindentation hardness and young's modulus.—Nanoindentation studies were performed to characterize the effects of hydrogen gas and substrate temperature on Young's modulus and hardness of BCN thin films, as shown in Fig. 3. Young's modulus of BCN thin films peaked at 140 GPa for the gas ratio of 0.2. With the increase in hydrogen gas, Young's modulus dipped to 126 GPa for the gas ratio of 0.6. For gas ratios higher than 0.6, Young's modulus is slightly increasing. Young's modulus showed an overall reducing trend with more hydrogen gas. This reduction in Young's modulus arises from the sp^2 to sp^3 transitions when H atoms are bonded with B/C/N atoms and has been reported in the past.[40,41] Young's modulus reduced from 132 GPa to 125 GPa for the films deposited at 200 °C as a function of substrate temperature. When the substrate temperature was higher than 200 °C, Young's modulus of the films followed an increasing trend, with the highest value of 140 GPa recorded for the film deposited at 400 °C. At higher temperatures, the films have higher Young's modulus and hardness values.

BCN film hardness values followed a decreasing trend for gas ratios of 0, 0.2, and 0.4 with the lowest hardness recorded at 6 GPa. Beyond that, the hardness values increased with higher hydrogen gas ratio. The films demonstrated the highest hardness value of 18 GPa for the gas ratio of 1. The increase in the hardness values can be attributed to the phase transitions in the films with varying hydrogen gas ratios as revealed from FTIR spectra. BCN films exhibited high hardness values as a function of substrate deposition temperature. The hardness of the films increased from 18 GPa for the film deposited at RT to 22 GPa for the film deposited at 400 °C. Enhancement in hardness with substrate temperature (22 GPa at 400 °C) was superior compared to hardness facilitated by the varying gas ratio (18 GPa for gas ratio 1). This increment in hardness stemmed from the increase in carbon and nitrogen content with substrate temperature and is attributed to characteristic C-N hard phases in the films.[7] Even though hydrogenation of dielectric

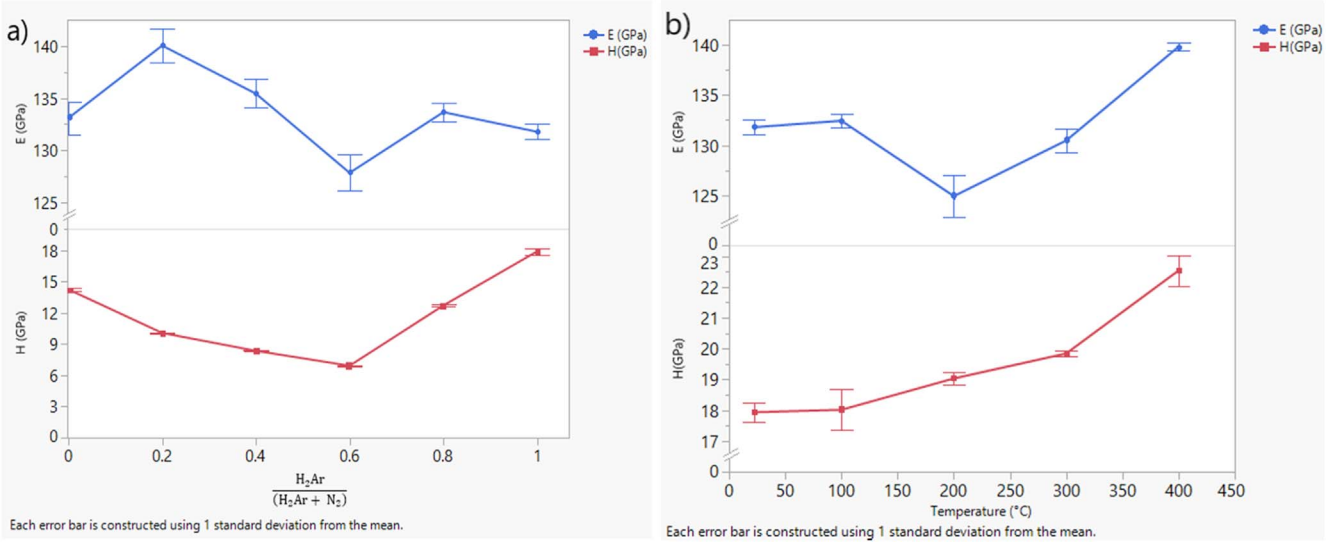

Figure 3. Young's modulus and hardness of BCNH thin films as a function of (a) gas ratio and (b) substrate temperature.

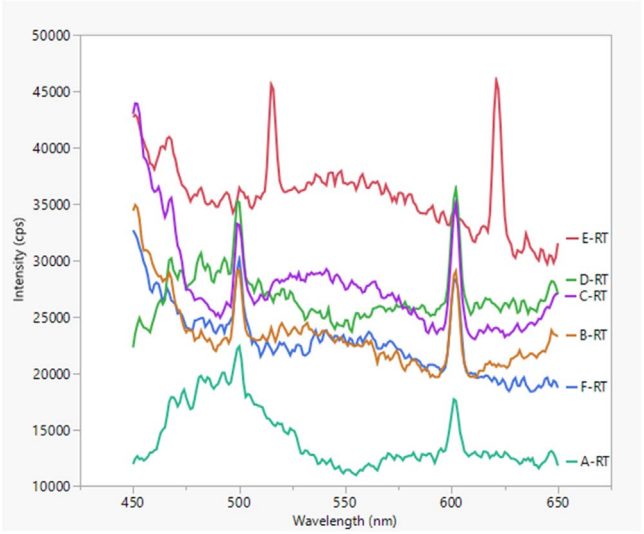

Figure 4. PL spectra of BCNH thin films as a function of hydrogen gas addition.

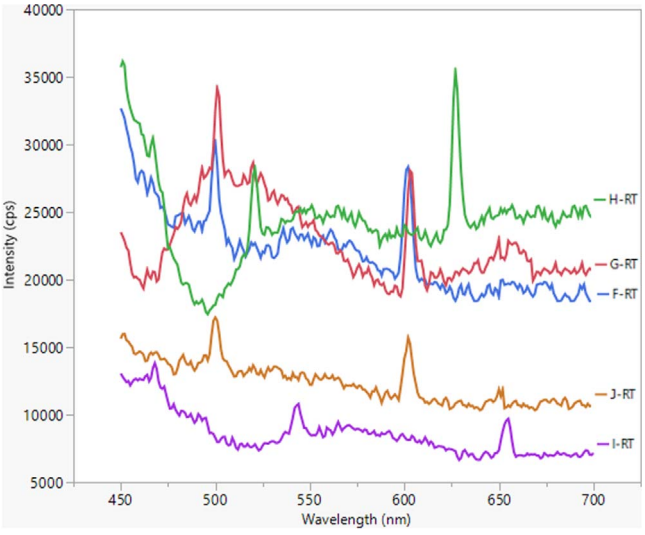

Figure 5. PL spectra of BCNH thin films as a function of substrate deposition temperature.

materials is known to negatively impact the mechanical properties of films due to increased porosity, hydrogenated boron carbon nitride films deposited in this study showed higher hardness values (18–22 GPa) compared to pure boron carbon nitride film (14 GPa).

Photoluminescence study.—Photoluminescence properties of BCNH thin films were examined under 365 nm excitation. The table shows the PL peak and corresponding bandgap energy for BCN and BCNH films. Two distinct PL peaks were observed for all films, as shown in Figs. 4 and 5. Film A, which is pure BCN thin film, exhibited two peaks at 490 nm (2.53 eV) and 591 nm (2.1 eV) with comparatively lower intensity. Similar peaks have been reported in BCN-based phosphors synthesized using different methods.[25,42,43] Films B, C, D, F exhibited a slight peak shift to 499 nm and 602 nm and sharper PL intensity with hydrogen gas. Film E displayed the highest peak intensity and a large peak shift to 515 nm and 621 nm. The composition of BCN films with different hydrogen to nitrogen gas ratios helps attain tunable films from 490 nm to 515 nm (blue to green shift) and from 591 nm to 621 nm (yellow to near-red shift). Table II shows that the PL intensity tends to increase with hydrogen concentration. This PL intensity enhancement due to hydrogen is primarily due to saturation of non-radiative recombination sites, such as dangling bonds.[44] Films A-C, D-E exhibited ~10,000 units higher PL intensity with a higher hydrogen gas ratio. This increase in PL intensity with hydrogen gas shows potential for hydrogen sensing applications of BCNH thin films and should be further explored. With the current demand for clean energy alternatives, hydrogen use will be critical towards the development of sustainable energy sources and applications. Hydrogen gas detection needs to be a priority to avoid hazards. BCNH thin films provide an added advantage of being able to operate at room temperature, good mechanical properties and can withstand harsh temperatures, unlike commercially used gas sensing materials such as ZnO, NiO, SnO_2, Fe_2O_3.[45]

PL properties of BCN films as a function of substrate deposition temperature are shown in Fig. 5. It is evident that with increasing substrate temperature, the PL peaks shifted to longer wavelengths. Film F deposited at RT exhibited peaks at 490 nm and 591 nm. As the substrate temperature increased, the peaks shifted to 521 nm and 627 nm for the film G deposited at 100 °C, 521 nm and 627 nm for the film H deposited at 200 °C, 544 nm and 655 nm for the film I deposited at 300 °C. Substrate temperature impacts the elemental composition indicating a slight increase in carbon content of the films as confirmed from EDS. The origin of PL peak shift to longer wavelength is due to the increase in the carbon content, which causes decrease in the bandgap.[46] BCN-based phosphors with a red emission peak up to 630 nm have been reported recently.[42] However, BCNH films deposited at the substrate temperature of 300 °C exhibited a sharp red emission peak up to 655 nm for the first time. The facile preparation and unique PL properties of BCN films with strong red peaks observed in this study make them promising candidates for potential applications in LEDs, optoelectronic devices, and bioimaging.

BCNH thin films deposited in this study exhibited a rare phenomenon of negative thermal quenching (NTQ). Figure 6 shows the PL behavior of BCNH thin films at RT and extremely low temperature (77 K). The NTQ phenomenon was observed only in films B, C, D, and E, which have both hydrogen and nitrogen doping. Pure BCN film did not exhibit the NTQ phenomenon. In conventional semiconductors, the luminescence intensity tends to decrease with temperature, widely known as thermal quenching (TQ). This mechanism is attributed to the temperature-induced increase in the non-radiative recombination probability of the PL emission. However, certain semiconductors exhibit an exact opposite mechanism of increasing luminescence intensity with temperature, termed as negative thermal quenching (NTQ). The NTQ phenomenon is commonly observed in materials like ZnO, ZnS, and GaAs.[47] The TQ and NTQ mechanism can be explained by the model proposed by Shibata et al.[48] For material with only two states, the initial state and final state, the thermal excitation of electrons from final to initial state is negligible if the energy separation between these two states is sufficiently large compared to the system temperature. However, materials can obtain multiple states between the initial and final states. For a multilevel system, the thermal excitation between the initial and plural middle states is not negligible since the separation is comparable to the temperature of the system. As a result, an increase in temperature is accompanied by an increase in luminescence intensity. Considering the fact that only films with both hydrogen and nitrogen doping exhibited NTQ, this emission can be associated with radiation recombination through localized states related to H and N atoms. Two-dimensional carbon and graphene quantum dots have been reported to exhibit NTQ phenomenon.[49] The presented data demonstrate the temperature-dependent characteristics of BCNH thin films and presents opportunities for future exploration of its optical properties. BCNH thin films deposited in this study exhibiting the NTQ phenomenon are attractive for selective and tunable optical emitters in the visible region, making them suitable for biomarkers and optical thermometry applications.

Table II. PL peaks with corresponding intensity and bandgap energy for all films.

Film	$H_2Ar/(H_2Ar+N_2)$	Deposition Temperature °C	PL peak 1 nm	Peak 1 intensity	PL peak 2 nm	Peak 2 intensity	Bandgap 1 eV	Bandgap 2 eV
A	0	RT	490	19063	591	12521	2.53	2.1
B	0.2	RT	500	29163	602	29058	2.48	2.06
C	0.4	RT	499	33249	602	35114	2.48	2.06
D	0.6	RT	499	35260	602	36366	2.48	2.06
E	0.8	RT	515	45594	621	45965	2.41	1.99
F	1.0	RT	499	29155	602	28336	2.48	2.06
G	1.0	100 °C	501	34166	603	28070	2.47	2.05
H	1.0	200 °C	521	28248	627	35441	2.38	1.98
I	1.0	300 °C	544	10802	655	9701	2.38	1.89

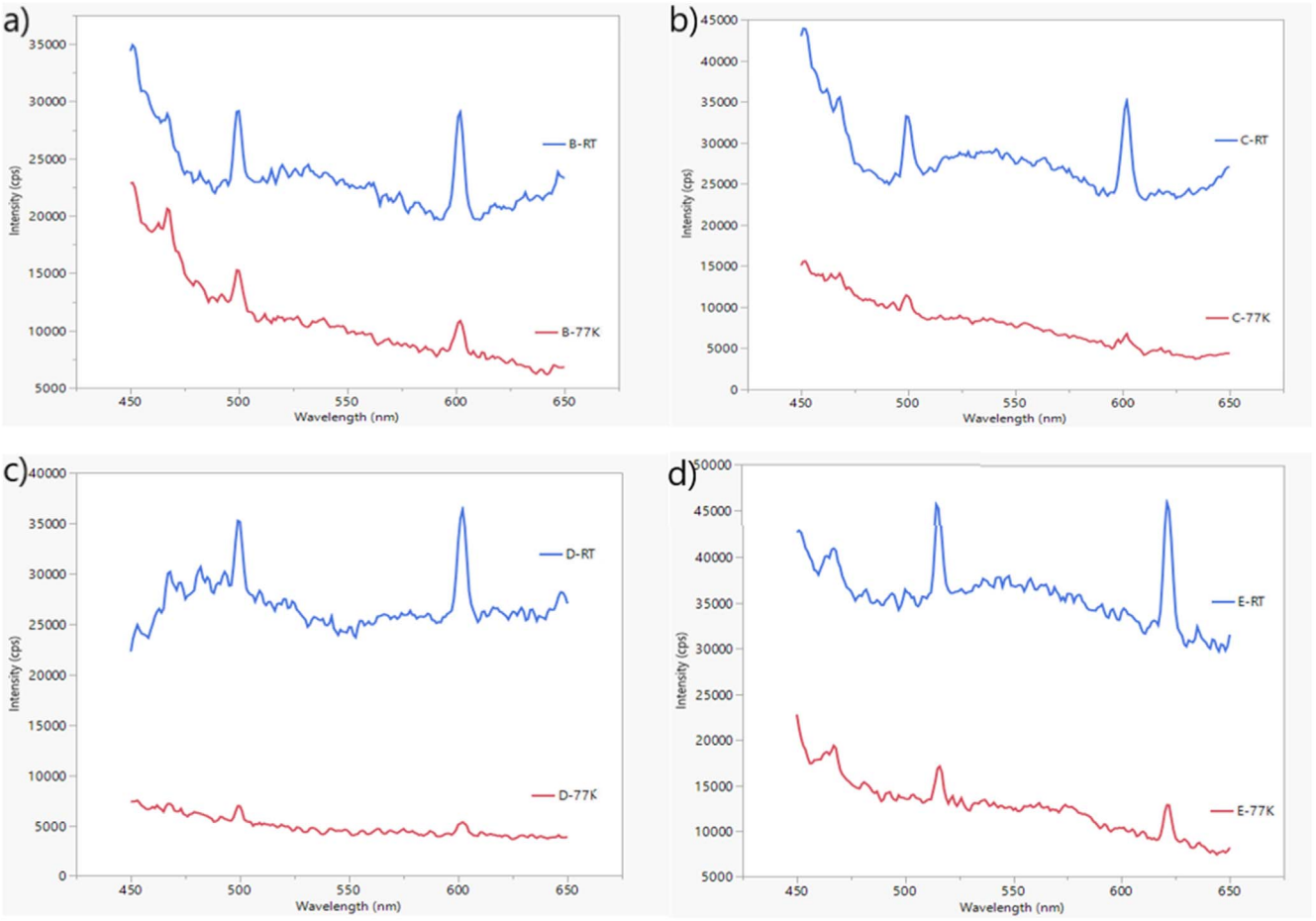

Figure 6. PL spectra of (a) film B (b) film C (c) film D, and (d) film E at room temperature (RT) and 77 K exhibiting the rare negative thermal quenching phenomenon.

Conclusions

Hydrogenated BCN thin films were deposited using dual-target RF sputtering from B_4C and BN targets. The hydrogen/argon to nitrogen gas ratio was varied while the substrate temperature was kept constant at room temperature to obtain films with diverse elemental compositions. In the next set, the hydrogen/argon to nitrogen gas ratio was set constant at 1, and the substrate temperature was varied from RT to 400 °C. BCN films can be tuned by varying the hydrogen/argon to nitrogen gas ratio and substrate temperature. The following conclusions were obtained from nanoindentation and PL studies.

1. Boron content increased with a higher hydrogen/argon gas ratio with maximum recorded as 35% at a gas ratio of 1. Carbon content varied slightly. Nitrogen content displayed an overall reducing trend, except the increase in content to 25% observed for the gas ratio of 0.8. Variation in substrate temperature produced boron-rich BCNH films. Carbon and nitrogen content increased at higher substrate temperature. Oxygen contamination was less than 10% for films deposited at higher substrate temperature. FTIR revealed the presence of B–N–B, C–N, C≡N, B–H, and C=O peaks in the transmission spectra.
2. While Young's modulus displayed a decreasing trend as a function of gas ratio variation, hardness values of films increased from 14 to 18 GPa at a higher gas ratio. Both Young's modulus and hardness displayed an overall increasing trend with substrate temperature.
3. Increasing amount of hydrogen gas helped attain tunable films with PL peak varying from 490 nm to 515 nm (green shift) and from 591 nm to 621 nm (near-red shift). With an increase in substrate temperature, PL peaks shifted to longer wavelengths. BCN-based phosphors up to 655 nm have been reported for the first time. A rare NTQ phenomenon was observed in some BCNH films related to radiation recombination through localized states of H and N atoms. BCN films reported in this study emit bright and stable red, green, and blue (RGB) luminescence peaks under a single excitation wavelength of 365 nm, making them potentially promising in numerous applications, such as light-emitting diodes, optoelectronic devices, bioimaging and optical thermometry.

References

1. H. Katsui, K. Harada, N. Kondo, and M. Hotta, "Preparation of boron carbon oxynitride phosphor film via laser chemical vapor deposition and annealing." *Surf. Coat. Technol.*, **394**, 125851 (2020).
2. X. Duan, Z. Yang, L. Chen, Z. Tian, D. Cai, Y. Wang, D. Jia, and Y. Zhou, "Review on the properties of hexagonal boron nitride matrix composite ceramics." *J. Eur. Ceram. Soc.*, **36**, 3725 (2016).
3. M. Keunecke, E. Wiemann, K. Weigel, S. Park, and K. Bewilogua, "Thick c-BN coatings–Preparation, properties and application tests." *Thin Solid Films*, **515**, 967 (2006).
4. K. Watanabe and T. Taniguchi, "Hexagonal boron nitride as a new ultraviolet luminescent material and its application." *Int. J. Appl. Ceram. Technol.*, **8**, 977 (2011).
5. T. Yuki, S. Umeda, and T. Sugino, "Electrical and optical characteristics of boron carbon nitride films synthesized by plasma-assisted chemical vapor deposition." *Diamond Relat. Mater.*, **13**, 1130 (2004).
6. T. Sugino, Y. Etou, T. Tai, and H. Mori, "Dielectric constant of boron carbon nitride films synthesized by plasma-assisted chemical-vapor deposition." *Appl. Phys. Lett.*, **80**, 649 (2002).
7. Z. Wu, Y. Wang, S. Li, X. Wang, Z. Xu, and F. Zhou, "Mechanical and tribological properties of BCN coatings sliding against different wood balls." *Science and Engineering of Composite Materials.*, **26**, 402 (2019).

8. V. Linss, S. Rodil, P. Reinke, M. Garnier, P. Oelhafen, U. Kreissig, and F. Richter, "Bonding characteristics of DC magnetron sputtered B–C–N thin films investigated by Fourier-transformed infrared spectroscopy and X-ray photoelectron spectroscopy." *Thin Solid Films*, **467**, 76 (2004).
9. N. Laidani, M. Anderle, R. Canteri, L. Elia, A. Luches, M. Martino, V. Micheli, and G. Speranza, "Structural and compositional study of B–C–N films produced by laser ablation of B4C targets in N2 atmosphere." *Appl. Surf. Sci.*, **157**, 135 (2000).
10. H. Yasui, Y. Hirose, K. Awazu, and M. Iwaki, "The properties of BCN films formed by ion beam assisted deposition." *Colloids Surf., B*, **19**, 291 (2000).
11. T. Sugino and H. Hieda, "Field emission characteristics of boron carbon nitride films synthesized by plasma-assisted chemical vapor deposition." *Diamond Relat. Mater.*, **9**, 1233 (2000).
12. S. Umeda, T. Yuki, T. Sugiyama, and T. Sugino, "Boron carbon nitride film with low dielectric constant as passivation film for high speed electronic devices." *Diamond Relat. Mater.*, **13**, 1135 (2004).
13. C. Wang, J. Xiao, Q. Shen, and L. Zhang, "Bonding structure and mechanical properties of BCN thin films synthesized by pulsed laser deposition at different laser fluences." *Thin Solid Films*, **603**, 323 (2016).
14. S. Xu, X. Ma, H. Wen, G. Tang, and C. Li, "Effect of annealing on the mechanical and scratch properties of BCN films obtained by magnetron sputtering deposition." *Appl. Surf. Sci.*, **313**, 823 (2014).
15. A. Prakash, S. D. Nehate, and K. B. Sundaram, "Boron carbon nitride based metal-insulator-metal UV detectors for harsh environment applications." *Opt. Lett.*, **41**, 4249 (2016).
16. S. Nehate, A. Saikumar, A. Prakash, and K. Sundaram, "A review of boron carbon nitride thin films and progress in nanomaterials." *Materials Today Advances.*, **8**, 100106 (2020).
17. J. Houska, P. Steidl, J. Vlcek, and J. Martan, "Thermal, mechanical and electrical properties of hard B4C, BCN, ZrBC and ZrBCN ceramics." *Ceram. Int.*, **42**, 4361 (2016).
18. V. Ivashchenko, V. Rogoz, T. Koltunowicz, and A. Kupchishin, *Microstructure and Mechanical Properties of Multilayered α-AlN/α-BCN Coatings Depending on Flux Density During Target B4C Sputtering. Advances in Thin Films, Nanostructured Materials, and Coatings* (Springer, Berlin) p. 51 (2019).
19. I. Karbhal, R. R. Devarapalli, J. Debgupta, V. K. Pillai, P. M. Ajayan, and M. V. Shelke, "Facile green synthesis of BCN nanosheets as high-performance electrode material for electrochemical energy storage." *Chemistry–A European Journal.*, **22**, 7134 (2016).
20. H. Tabassum, C. Qu, K. Cai, W. Aftab, Z. Liang, T. Qiu, A. Mahmood, W. Meng, and R. Zou, "Large-scale fabrication of BCN nanotube architecture entangled on a three-dimensional carbon skeleton for energy storage." *J. Mater. Chem. A*, **6**, 21225 (2018).
21. I. Karbhal, A. Basu, A. Patrike, and M. V. Shelke, "Laser patterning of boron carbon nitride electrodes for flexible micro-supercapacitor with remarkable electrochemical stability/capacity." *Carbon*, **171**, 750.
22. S. Wang, F. Ma, H. Jiang, Y. Shao, Y. Wu, and X. Hao, "Band gap-tunable porous Borocarbonitride nanosheets for high energy-density supercapacitors." *ACS Appl. Mater. Interfaces*, **10**, 19588 (2018).
23. Z. Chen and M. Lu, "Thionine-coordinated BCN nanosheets for electrochemical enzyme immunoassay of lipocalin-2 on biofunctionalized carbon-fiber microelectrode." *Sensors Actuators B*, **273**, 253 (2018).
24. V. Naga, S. D. Nehate, A. K. Saikumar, and K. B. Sundaram, "Boron carbon nitride (BCN) nano-coatings of central venous catheters inhibits bacterial colonization." *ECS J. Solid State Sci. Technol.*, **9**, 115018 (2020).
25. T. Ogi, Y. Kaihatsu, F. Iskandar, W. N. Wang, and K. Okuyama, "Facile synthesis of new full-color-emitting BCNO phosphors with high quantum efficiency." *Adv. Mater.*, **20**, 3235 (2008).
26. R.-J. Xie, N. Hirosaki, N. Kimura, K. Sakuma, and M. Mitomo, "2-phosphor-converted white light-emitting diodes using oxynitride/nitride phosphors." *Appl. Phys. Lett.*, **90**, 191101 (2007).
27. R.-J. Xie, N. Hirosaki, Y. Li, and T. Takeda, "Rare-earth activated nitride phosphors: synthesis, luminescence and applications." *Materials.*, **3**, 3777 (2010).
28. M. Ren, W. Han, Y. Bai, C. Ge, L. He, and X. Zhang, "Melamine sponge-assisted synthesis of porous BCNO phosphor with yellow-green luminescence for Cr6 + detection." *Mater. Chem. Phys.*, **244**, 122673 (2020).
29. Y. Jian, Q. Tai, and S. Chun-Ying, "New BCN fibres for strong ultraviolet and visible light luminescence." *Chin. Phys. Lett.*, **23**, 2573 (2006).
30. X. Zhang, Z. Lu, J. Lin, L. Li, Y. Fan, L. Hu, X. Xu, F. Meng, J. Zhao, and C. Tang, "Luminescence properties of BCNO phosphor prepared by a green and simple method." *Mater. Lett.*, **94**, 72 (2013).
31. V. S. Sulyaeva, Y. M. Rumyantsev, V. G. Kesler, and M. L. Kosinova, "Synthesis and optical properties of BCxNy films deposited from N-triethylborazine and hydrogen mixture." *Thin Solid Films*, **581**, 59 (2015).
32. H. Aoki, T. Masuzumi, M. Hara, D. Watanabe, C. Kimura, and T. Sugino, "Effect of the radio-frequency power on the dielectric properties of hydrogen-containing boron carbon nitride films deposited by plasma-assisted chemical vapor deposition using tris (dimethylamino) boron gas." *Thin Solid Films*, **518**, 2102 (2010).
33. H. Aoki, T. Masuzumi, M. Hara, Z. Lu, D. Watanebe, C. Kimura, and T. Sugino, "Influence of the methyl group on the dielectric constant of boron carbon nitride films containing it." *Diamond Relat. Mater.*, **19**, 1437 (2010).
34. A. Prakash, V. Todi, K. B. Sundaram, L. Ross, G. Xu, M. French, P. Henry, and S. W. King, "Investigation of the dielectric and mechanical properties for magnetron sputtered BCN thin films." *ECS J. Solid State Sci. Technol.*, **4**, N3122 (2014).
35. A. Prakash, K. B. Sundaram, and A. D. Campiglia, "Photoluminescence studies on BCN thin films synthesized by RF magnetron sputtering." *Mater. Lett.*, **183**, 355 (2016).
36. T. Kida, K. Shigezumi, M. A. Mannan, M. Akiyama, Y. Baba, and M. Nagano, "Synthesis of boron carbonitride (BCN) films by plasma-enhanced chemical vapor deposition using trimethylamine borane as a molecular precursor." *Vacuum*, **83**, 1143 (2009).
37. M. Polo, E. Martinez, J. Esteve, and J. Andujar, "Preparation of B C N thin films by rf plasma assisted CVD." *Diamond Relat. Mater.*, **7**, 376 (1998).
38. F. Yang, M. Zhao, B. Zheng, D. Xiao, L. Wu, and Y. Guo, "Influence of pH on the fluorescence properties of graphene quantum dots using ozonation pre-oxide hydrothermal synthesis." *J. Mater. Chem.*, **22**, 25471 (2012).
39. T. Hasegawa, K. Yamamoto, and Y. Kakudate, "Influence of raw gases on B–C–N films prepared by electron beam excited plasma CVD." *Diamond Relat. Mater.*, **12**, 1045 (2003).
40. Q. Pei, Y. Zhang, and V. Shenoy, "A molecular dynamics study of the mechanical properties of hydrogen functionalized graphene." *Carbon*, **48**, 898 (2010).
41. J. F. Dethan and V. Swamy, "Tensile properties of hydrogenated hybrid graphene–hexagonal boron nitride nanosheets: a reactive force field study." *Mol. Simul.*, **46**, 1220 (2020).
42. X. Zhang, S. Yan, Y. Cheng, K. Gao, Z. Lu, F. Meng, J. Lin, X. Xu, J. Zhao, and C. Tang, "Spectral properties of BCNO phosphor with wide range of excitation and emission." *Mater. Lett.*, **102**, 102 (2013).
43. W.-N. Wang, T. Ogi, Y. Kaihatsu, F. Iskandar, and K. Okuyama, "Novel rare-earth-free tunable-color-emitting BCNO phosphors." *J. Mater. Chem.*, **21**, 5183 (2011).
44. B. Marchon, J. Gui, K. Grannen, G. C. Rauch, J. W. Ager, S. Silva, and J. Robertson, "Photoluminescence and Raman spectroscopy in hydrogenated carbon films." *IEEE Trans. Magn.*, **33**, 3148 (1997).
45. J. Dai, O. Ogbeide, N. Macadam, Q. Sun, W. Yu, Y. Li, B.-L. Su, T. Hasan, X. Huang, and W. Huang, "Printed gas sensors." *Chem. Soc. Rev.*, **49**, 1756 (2020).
46. K. Moses, S. N. Shirodkar, U. V. Waghmare, and C. Rao, "Composition-dependent photoluminescence and electronic structure of 2-dimensional borocarbonitrides, BC XN (x = 1, 5)." *Mater. Res. Express*, **1**, 025603 (2014).
47. M. Watanabe, M. Sakai, H. Shibata, C. Satou, S. Satou, T. Shibayama, H. Tampo, A. Yamada, K. Matsubara, and K. Sakurai, "Negative thermal quenching of photoluminescence in ZnO." *Physica B*, **376**, 711 (2006).
48. H. Shibata, "Negative thermal quenching curves in photoluminescence of solids." *Japan. J. Appl. Phys.*, **37**, 550 (1998).
49. T. Dey, S. Mukherjee, A. Ghorai, S. Das, and S. K. Ray, "Surface state selective tunable emission of graphene quantum dots exhibiting novel thermal quenching characteristics." *Carbon*, **140**, 394 (2018).